

Beryllium doubly excited autoionizing resonances between the $2p$ and $3p$ thresholds

P. Olalde-Velasco, E. Méndez-Martínez,* and J. Jiménez-Mier
Instituto de Ciencias Nucleares, UNAM, 04510 Mexico DF, Mexico

R. Wehlitz

Synchrotron Radiation Center, University of Wisconsin-Madison, Stoughton, Wisconsin 53589, USA

S. B. Whitfield

Department of Physics and Astronomy, University of Wisconsin-Eau Claire, Eau Claire, Wisconsin 54702, USA

(Received 5 July 2007; published 5 September 2007)

We present results of high resolution photoelectron spectrometry measurements for the $\sigma(2s)$ relative partial photoionization cross section between the $2p$ and $3p$ ionization thresholds in atomic beryllium. This includes the $3snp$ autoionizing resonance series converging to the $3s$ threshold, the $3pns$, nd series converging to the $3p$ threshold, and several members of the $3dnp$, nf series. The results for the perturbed $3snp$ series are compared with the ion yield results that give the total photoionization cross section. We found very good agreement with calculations for the $2s$ partial cross section both in the R -matrix approximation and a hyperspherical calculation. We confirm the perturbation of the series by the $3p4s$ interloper with a resonance profile that is the same as for the total cross section. We did not find evidence of a second interloper ($3d4p$) between the $3s10p$ and $3s11p$ resonances. We also find very good agreement between experiment and theory for the Shore parameters of these resonances. The data for the resonances between the $3s$ and $3p$ thresholds are compared with the results of a R -matrix $2s$ cross section calculation. Good agreement is found for the energy positions and overall resonance shapes once the calculated energies are referred to the experimental $3p$ threshold.

DOI: [10.1103/PhysRevA.76.032701](https://doi.org/10.1103/PhysRevA.76.032701)

PACS number(s): 32.80.Dz, 32.80.Fb

I. INTRODUCTION

Beryllium is the simplest atom with two closed shells. However, compared to helium it has only been studied marginally. Due to its relative simplicity, Be is an excellent test case for atomic theory as it can be treated in a rigorous manner [1]. Because of this several groups have performed a wide variety of calculations [2–12]; some of them include multiconfiguration interactions to calculate fluorescence yields [2], photoionization cross section in the inner shell [3,4], and in the region of the doubly excited states [5–12].

In the past not much experimental research has been conducted on Be atoms mainly because of its low vapor pressure even at relatively high temperatures. Despite this, there have been photoionization experiments that provide valuable information about the effect of electronic correlation in this atom. Among these there are beam foil spectroscopy experiments [13], absorption measurements using a vacuum spark [14,15], two laser plasma source experiments [16,17], ion yield experiments looking for single and double photoionization [18–25], and Auger [1] and photoelectron [26–28] experiments using synchrotron radiation.

Considering only single photoionization measurements using synchrotron radiation, the experiments can be separated into two main types: those that involve inner shell excitations [26–28] and the experiments dealing with photoionization of the valence electrons in the region of the double excited states. This region was studied first in the absorption

measurements using a vacuum spark [14] and recently with synchrotron radiation by ion yield experiments [19,22]. All this research was done with excitation energies up to the $3s$ threshold (20.26172 eV [29]).

Wehlitz *et al.* [19] were the first to measure the resonance parameters of the $2pns$ ($n=3-8$) and $2pnd$ ($n=3-5$) doubly excited states converging to the $2p$ threshold. From their measured energies they derived the corresponding quantum defects for the ns and nd series. Recently, Yoshida *et al.* [22] reported ion yield experiments for the doubly excited resonances between the Be^+2p and $3s$ thresholds. In this region theory predicts that the main $3snp$ series is perturbed by several interlopers, but they only could observe the strong perturbation of the $3snp$ series by the $3p4s$ resonance. These ion yield experiments are in good agreement with earlier absorption measurements [14], with the total cross section results obtained in an R -matrix calculation [12], and also with a hyperspherical calculation [11].

In this work we present high resolution photoelectron spectrometry measurements for the $2s$ relative partial photoionization cross section in the region of the doubly excited resonances between the $2p$ and $3p$ thresholds. We compare our results between the $2p$ and $3s$ thresholds with the ion yield data of Yoshida *et al.* [22] and also with the $2s$ partial cross section calculations obtained in both a hyperspherical calculation [11] and an R -matrix calculation [12]. Our better resolution allowed us to obtain data up to the $3s11p$ resonance, in a region where theory [11,12] predicts the presence of an interloper ($3d4p$). We give results for the resonance parameters (resonance energy, width, and Shore parameters) for this series. The Shore parameters [30] give additional information about the coupling between the resonant state

*Present address: Facultad de Ciencias, Universidad Autónoma del Estado de México, Toluca, Estado de México, México.

and the partial wave continua [31]. We present results for the quantum defects of all members of the $3snp$ series up to $n = 11$.

We also extended these $2s$ photoelectron measurements to the $3p$ threshold. In this region theory [12] predicts several resonances converging to the $3p$ and to the $3d$ thresholds. We make a qualitative comparison of our results with the R -matrix $2s$ partial cross section calculation [12].

These results for the $2s$ partial photoionization cross section should complement the lower resolution ion yield results [22] that give information about the total cross section. A comparison between the two provides important information about partial photoionization cross sections of unobserved open channels such as the $2pk\ell$.

It is our intention that our results will stimulate further investigations on this region and also to contribute to a better understanding of electronic correlation in this simple atomic system.

II. EXPERIMENT

The experiment was conducted in two separate runs at the University of Wisconsin Synchrotron Radiation Center using a bending magnet beamline and an undulator beamline. In the first run the photons were monochromatized by a 1200 lines/mm gold coated concave grating ($R=998.9$ mm) mounted in a stainless steel Seya Namioka (SS-Seya) monochromator [32]. In the second run a 1200 lines/mm gold coated plane grating monochromator (PGM) was used [33]. The monochromatized photons were then directed through a glass capillary into the interaction region. The Be cloud was produced by a resistively heated tantalum crucible, which contained small pieces of beryllium wire (purity greater than 99.9%). In this experiment we used both the “internal” and the “external” oven arrangements [34]. In the external oven configuration the effusive atomic vapor produced by the crucible flows into a source cell where the interaction with the incoming radiation occurs. For the internal oven arrangement the crucible serves also as the photoelectron source. The internal oven crucible has two slits facing perpendicular directions that allow the photoelectrons to pass directly into the analyzers while for the external oven the slits are on the copper cell. The electrostatic analyzers are mounted on a platform perpendicular to the photon beam making angles of 0° and 90° with respect to the polarization vector of the synchrotron radiation. These analyzers have a nominal resolution of 1% of the pass energy. Both ovens were typically operated at a power of 190 W, corresponding to a crucible temperature of about 1230 °C. The pressures inside the copper cell and the internal oven were estimated to be 1.2×10^{-3} and 1.2×10^{-2} torr, respectively. In this setup we were able to follow the $\text{Be}^+(2s)$ photoelectron signal at both 0° and 90° with respect to the polarization vector of the ionizing radiation. This polarization was determined by the angular distribution of known calibrant noble gases and was assumed to be constant throughout the entire energy region. We measured a polarization of 0.99(5) for the PGM beamline and 0.91(4) for the SS-Seya beamline. The complete absence of the photoelectron beryllium $2s$ signal above the back-

ground at 90° confirmed that for beryllium $\beta_{2s}=2.0$ [35] even across the autoionizing resonances [36].

Photoelectron spectra were collected in two different modes: the photoelectron-spectrometry (PES) mode, in which the electron intensity is recorded as a function of the electron kinetic energy at a fixed photon energy, and the constant-ionic-state (CIS) mode in which spectra are recorded by simultaneously scanning the incident photon energy and the accelerating or retarding voltage of the source cell (crucible) so as to always observe electrons that correspond to the same final ionic state. The resolution of a CIS spectrum depends solely on the bandpass of the monochromator. The resolution of the electron spectrometer only plays a role insofar as it must be capable of isolating single final states of the ion, which is the case for the $2s$ state of Be^+ . The bandpass of both beamlines was determined using the $\text{Kr}4p_{3/2}$ autoionizing resonances. First we determined the instrumental contribution to the width of the $8s$ resonance at 14.097 eV [37], then we assumed a constant bandpass in wavelength and extrapolated its value to a photon energy of 20.7 eV. At this photon energy we obtained 27.5(1.0) and 7.5(5) meV for the SS-Seya and PGM beamlines, respectively. The latter bandpass is a factor of 4 better than the one used in the ion yield experiments [22].

The energy region studied in this experiment goes from 17.25 to 21.34 eV. As this region is between the $2p$ and $3p$ thresholds the open channels are $2s$, $2p$, and $3s$. However, the high background for low energy electrons prevented us from measuring any channels except the $2s$. For convenience the entire region was separated into two smaller ones, the first from 17.25–20.34 eV and the second from 20.29–21.34 eV. Both regions were studied first on the SS-Seya beamline in 15 meV steps and in 5 meV steps, respectively. Later on a portion of both regions, ranging from 19.52–20.24 eV and from 20.22–21.02 eV was studied with 5 meV steps and a better resolution in the PGM beamline. In the overlap regions at least 5 points make it possible to “stitch” the separate CIS scans together.

The energy interval for the PGM run is rather small, about 1.7 eV. To calibrate the energy scale in this case we performed a quantum defect analysis of the beryllium $3snp$ resonances, with the resonance energies measured directly from the beamline (i.e., with no correction applied). As a result of this analysis we obtained the $3s$ limit, which is then compared with the value of 20.262 072 eV reported by NIST [29]. We found that all of our resonance energies had to be shifted up by 9 meV to obtain this limit.

The energy interval of the SS-Seya run covers a wider range. To calibrate the photon energy of this run we used the $\text{Kr}4p_{3/2}$ autoionizing resonances at the low energy end, and the beryllium $3snp$ resonance positions from the PGM run for the high energy end. We estimate that our overall photon energy scale is accurate to within 3 meV.

In Table I we present the relevant ionization thresholds relative to the ground state of atomic Be that were used in this work [29]. We also compare this value with the results of the R -matrix [12] and hyperspherical [11] calculations.

Changes in the photon flux during the course of the CIS scans were monitored by simultaneously recording the current output of a 90% transmission Ni mesh just beyond the

TABLE I. Energy levels relative to the ground state of atomic Be.

| Ionic state | Energy level (eV) | | |
|----------------------|-------------------|---------------------|---------------------|
| | NIST ^a | Theory ^b | Theory ^c |
| Be II $1s^2 2s(^2S)$ | 9.322699 | 9.2959 | |
| Be II $1s^2 2p(^2P)$ | 13.281902 | 13.2543 | |
| Be II $1s^2 3s(^2S)$ | 20.262072 | 20.2305 | |
| Be II $1s^2 3p(^2P)$ | 21.286757 | 21.2688 | |
| Be III $1s^2(^1S)$ | 27.533852 | | 27.5586 |

^aFrom Ref. [29].

^b R -matrix result from Ref. [12].

^cHyperspherical result from Ref. [11].

final optics of both beamlines. A detailed explanation of how this and other calibrations were employed to correct the CIS spectra for changes in the oven yield and the influence of the background are given elsewhere [38]. After applying these procedures each CIS spectrum corresponds to a $2s$ relative cross section for the $\text{Be}^+(2s)$ ionic channel. We then multiply the photoelectron intensity by a constant factor in order to compare this relative cross section to the calculated $2s$ partial cross section [11,12]. We decided to minimize the quadratic deviations of our data from the R -matrix results [12] in the region covered by the PGM data. The multiplicative factor is therefore the ratio of the average cross section divided by the average counts per point in this energy region. We found that this multiplicative factor was also adequate to compare with the hyperspherical data [11].

III. RESULTS AND DISCUSSION

An overall view of the results of our measurements for the autoionizing resonances between the $2p$ and $3s$ threshold in the $\text{Be}^+(2s)$ ionic channel is presented in the lower panel of Fig. 1. Here we make a comparison between the data obtained in the SS-Seya run, with a 27.5 meV resolution, covering the energy region up to 19.5 eV, and the data of the PGM run, with a 7.5 meV resolution, covering the region between 19.5 eV and the $3s$ threshold. The data are all corrected for the transmission of the monochromator, and the energies were shifted according to the procedure described in Sec. II. For this plot we convoluted both theoretical data sets with triangular window functions whose widths are 27.5 eV between 17 and 19.5 eV, and 7.5 eV between 19.5 eV and the $3s$ threshold. The original energy scale of the R -matrix results [12] was shifted upward by 31.6 meV so that all results are referred to the NIST $3s$ ionic threshold in Table I. The hyperspherical energy scale is originally relative to the Be^{2+} threshold. We took its value from NIST [29] in Table I.

At the top panel of Fig. 1 we make a similar comparison between the ion yield data of Yoshida *et al.* [22] and the total cross section calculations. In this case the theoretical values were convoluted with instrument window functions whose widths were 36 meV for the first two resonances and 32 meV for the rest of the series converging to the $3s$ thresh-

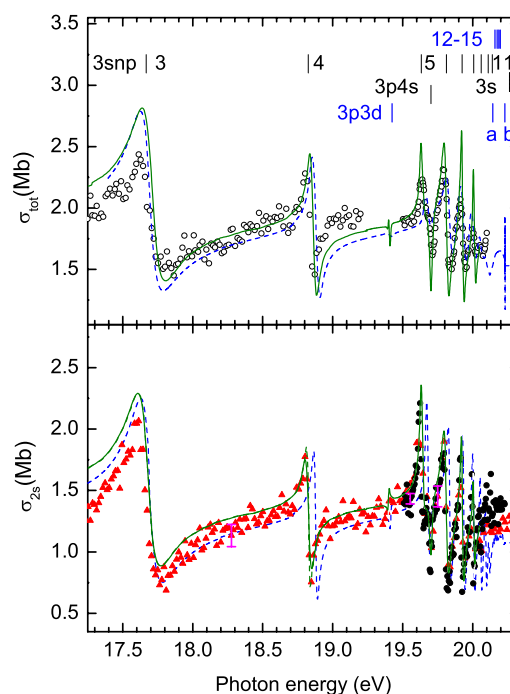


FIG. 1. (Color online) $3snp$ autoionizing resonances between the $2p$ and $3s$ threshold in atomic beryllium. Lower panel: $2s$ partial photoionization cross section. Solid triangles (red): CIS spectrum of the SS-Seya run (see text). Filled circles (black): CIS spectrum of the PGM run. Also shown are typical error bars (magenta) for both sets of data. Dashed line (blue): R -matrix calculation [12] for the $2s$ partial cross section convoluted with a 7.5 meV instrument window function. Solid line (green): hyperspherical calculation [11] convoluted with a 7.5 meV window function. Upper panel: total cross section. Open circles (black): ion yield results [22]. Dashed line (blue): R -matrix results [12] convoluted with a 36 meV instrument window function. Solid line (green): hyperspherical results [11] convoluted with a 36 meV instrument window function. The resonance energies are indicated by vertical lines as indicated in the text. The calculated [12] position of resonances $3d4p$ and $3d4f$ is indicated by a and b , respectively.

old. These are the experimental widths determined in the ion yield experiment [22]. There is a very clear correspondence between our photoelectron measurements for the $2s$ partial cross section and the lower resolution ion yield results [22] that give the total ionization cross section. In both cases there is also very good agreement with theory. The energy position of the $3snp$ up to $n=11$ and the $3p4s$ interloper in Fig. 1 are taken from our data; the higher $3snp$ members ($n=12-15$), the $3p3d$, $3p4s$, and $3d4p$ were taken from the R -matrix results shifted up by 31.6 meV. The $3s$ threshold is taken from NIST [29].

The calculations predict the presence of a first interloper, resonance $3p3d$, at about 19.40 eV. It appears as a window in the total cross section and more like an asymmetric profile in the $2s$ partial cross section. The scatter in our experimental data did not allow us to observe it. This was also the case for the ion yield experiment [22].

A more detailed view of the region between 19.5 and 20.25 eV is presented in Fig. 2. Once again, in the lower panel we show our $2s$ photoelectron results and in the upper

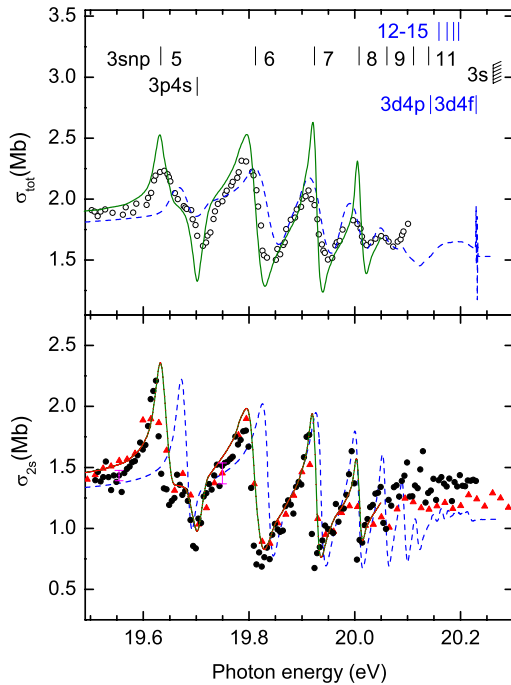


FIG. 2. (Color online) Detail of $3snp$ autoionizing resonances in atomic beryllium. Lower panel: $2s$ partial photoionization cross section. Solid triangles (red): CIS spectrum of the SS-Seya run (see text). Filled circles (black): CIS spectrum of the PGM run. Also shown are typical error bars (magenta) for both sets of data. Dashed line (blue): R -matrix calculation [12] for the $2s$ partial cross section convoluted with a 7.5 meV instrument window function. Solid line (green): Hyperspherical calculation [11] convoluted with a 7.5 meV window function. Upper panel: total cross section. Open circles (black): ion yield results [22]. Dashed line (blue): R -matrix results [12] convoluted with a 36 meV instrument window function. Solid line (green): hyperspherical results [11] convoluted with a 36 meV instrument window function. The resonance energies are indicated by vertical lines as indicated in the text.

panel the ion yield results of Yoshida *et al.* [22]. Both experimental data sets seem to favor the hyperspherical calculation [11] over the R -matrix results [12]. This is particularly clear in the region of the $3s5p$ resonance and the $3p4s$ interloper around 19.65 eV. The experimental data give two well separated structures, with a positive excursion peak at 19.632 eV and a pronounced dip at 19.707 eV. The R -matrix calculation [12] predicts that as a result of the interaction between the two states the cross section appears as a narrow, weak dispersion-like profile. The hyperspherical calculation [11] gives two separated structures with the right overall shape but smaller energy separation, with the dip appearing at a lower energy compared to the experimental one. For resonance $3s6p$ our results and the ion yield results are in better agreement with the hyperspherical calculation in terms of both line shape and energy position. Here it is interesting to point out that theory predicts that the effect of the $3p4s$ interloper is to create a shoulder on the low energy side of the $6p$ resonance, at about 19.75 eV. This shoulder is clearly visible in both our $2s$ partial cross section measurement and in the ion yield results [22]. For the higher resonances the agreement between experiment and theory is, in general,

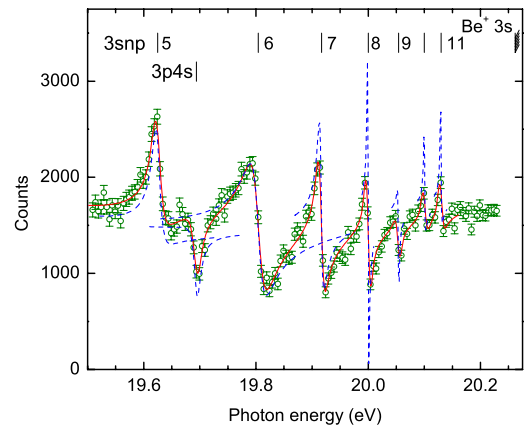


FIG. 3. (Color online) Fit of Shore profiles to the $\text{Be}^+(2s)$ relative photoionization cross section. Open circles (green): experimental data. Solid line (red): result of the Shore fit including a quadratic background. Dashed lines (blue): individual line profiles with the instrument width removed.

very good and about the same for the R -matrix [12] and the hyperspherical calculation [11]. In the energy region around 20.10 eV both calculations predict a second interloper, namely, the $3d4p$ resonance. In our data we do not see an indication of the presence of this resonance even though the variation in intensity of our data seems to slightly favor, again, the hyperspherical calculation [11]. Clearly the ion results do not have enough resolution to allow a precise identification of this state.

It is remarkable that the overall behavior in both the total cross section and the $2s$ partial cross section is the same. The difference in these two cross sections is due to contributions from the Be^+2p ionic channel, and the comparison we just made indicates that the effect of this channel is not as important at the resonances. This is in agreement with theory. Both calculations [11,12] predict that the $2pks$ and $2pkd$ partial cross sections have a mirroring [39,40] behavior that minimizes the variations of the $2p$ partial cross across the resonances. For instance, the calculations predict [11,12] that at the $3s3p$ resonance the $2p$ channel contribution to the total cross section is almost constant.

A much better indication of the presence of the higher energy interloper would show up in a fit of resonance profiles to the experimental data, and then in an analysis of the quantum defects of the whole series. We present the results of such a fit to our $2s$ photoelectron data in Fig. 3. We chose a Shore profile for each resonance according to [30]

$$\sigma = \frac{A\epsilon + B}{1 + \epsilon^2} + \sigma_c, \quad (1)$$

where $\epsilon = 2(E - E_0)/\Gamma$, and A and B are the Shore parameters, which are related to the real and imaginary part of the fraction of the dipole amplitude that passes through the only eigenchannel that interacts with the resonant state [31]. In this expression E is the excitation energy, E_0 is the energy position of the resonance, and Γ is the resonance width (FWHM). The term σ_c represents the nonresonant photoionization cross section. We also have to include the effect of

TABLE II. Comparison between experiment and theory for the Shore parameters of the $3snp$ resonances and the $3p4s$ interloper in beryllium.

| Resonance | Experiment ^a | | | | Theory ^b | | | | Theory ^c | | | |
|-----------|-------------------------|----------------|------------|------------|---------------------|----------------|----------|----------|---------------------|----------------|----------|----------|
| | E_0 (eV) | Γ (meV) | A (Mb) | B (Mb) | E_0 (eV) | Γ (meV) | A (Mb) | B (Mb) | E_0 (eV) | Γ (meV) | A (Mb) | B (Mb) |
| $3s3p$ | 17.654(8) | 161(7) | -0.555(15) | 0.132(30) | 17.654 | 148 | -1.405 | 0.333 | 17.683 | 149 | -0.143 | 0.403 |
| $3s4p$ | 18.818(4) | 12.4(3.1) | -0.85(23) | -0.055(85) | 18.810 | 10.95 | -2.38 | -0.189 | 18.879 | 19.97 | -1.20 | -0.039 |
| $3s5p$ | 19.625(3) | 17.3(1.0) | -0.75(18) | -0.07(14) | 19.619 | 23.2 | -0.664 | 0.918 | 19.675 | 20.0 | -0.433 | 0.769 |
| $3s6p$ | 19.804(3) | 28.7(1.6) | -1.213(57) | 0.013(24) | 19.791 | 31.8 | -1.225 | 0.166 | 19.837 | 20.9 | -1.248 | -0.148 |
| $3s7p$ | 19.917(3) | 8(2) | -1.49(15) | 0.35(14) | 19.908 | 11.2 | -1.511 | 0.356 | 19.937 | 18.2 | -1.314 | -0.033 |
| $3s8p$ | 20.000(3) | 2(2) | -2.95(97) | 0.37(39) | 19.990 | 2 | -2.667 | 0.765 | 20.008 | 13.9 | -1.146 | 0.084 |
| $3s9p$ | 20.054(3) | 2(3) | 0.79(26) | -0.51(33) | 20.043 ^d | | | | 20.058 | 10.7 | -0.923 | 0.171 |
| $3s10p$ | 20.100(3) | 2(3) | -0.80(28) | 0.55(38) | 20.094 ^d | | | | 20.094 | 8.5 | -0.631 | 0.244 |
| $3s11p$ | 20.130(3) | 2(3) | -0.83(31) | 0.80(34) | 20.123 ^d | | | | 20.117 | 4.9 | -0.192 | 0.157 |
| $3p4s$ | 19.694(3) | 13.9(2.4) | -0.303(80) | -0.562(95) | 19.683 | 15.6 | -0.029 | -0.538 | 19.690 | 13.7 | -0.186 | -0.451 |

^aThis work.^bResult of our fit to digitized hyperspherical data of Ref. [11].^cResult of our fit to R -matrix data of Ref. [12].^dWe took the resonance energy directly from Fig. 5 of Ref. [11].

the monochromator window function [41] in our data. We used a window function whose width is 27.5 meV for the SS-Seya data and a 7.5 eV bandpass window for the PGM data. A comparison among our results for this fitting procedure and the R -matrix calculation [12] and the hyperspherical calculation [11] is made in Table II. The parameters for the two calculations in this table were obtained from similar fits to the theoretical R -matrix data [12] or to our own digitization of the published results of the hyperspherical data [11].

The fit energies in Table II already show the correction due to the energy calibration. Our results are thus referred to the NIST value of the Be^+3s limit in Table I. The R -matrix parameters for the $3s3p$ to $3s11p$ were obtained from a fit we made to the $2s$ cross section data in Ref. [12]. The energy values were shifted up by 31.6 meV, which is the energy difference between the calculated and the experimental value for the thresholds in Table I. The hyperspherical data were taken directly from a digitization of the partial cross section plot in Ref. [11]. For this reason we could only fit the resonances up to $3s8p$. In this case the original energies were referred to the Be^{2+} limit, and we used for this the NIST value [29] in Table I.

Our resonance energies are consistently lower than the values found by Yoshida *et al.* in the ion yield experiment [22]. The mean difference between both sets of experimental results is -9 meV, which is larger than our expected uncertainty. Our energies are, however, in slightly better agreement with earlier spark absorption results [14]. Our measured widths are in good agreement with the values of the ion yield experiment [22]. At this point it is important to recall that the ion yield data were fitted to Fano profiles while we are using Shore profiles for our photoelectron data. In this regard it is important that no major discrepancies were found for the resonance energies and widths.

In Table II one can see that the agreement between experiment and theory for the results of our fit is very good.

The resonance energies in the hyperspherical calculation are slightly lower than the measured ones, the mean difference being -9 meV. On the other hand, there is a systematic trend in the difference between the experimental energies and the results of the R -matrix calculation. Starting at resonance $3s5p$ the difference grows linearly if one does not take into account the shift between experimental [29] and theoretical [12] values for the $3s$ threshold. In general there is fair agreement between experiment and both theories for the resonance widths. Except for the $3s6p$ and $3p4s$ resonances our measured widths are consistently lower than the calculated ones, and the discrepancy is beyond the quoted error. The lower values obtained for the experimental data for resonances $3s8p$ - $3s11p$ are mainly due to the difficulty in the fit procedure. The agreement between experiment and theory for the other two Shore parameters, namely, A and B is really remarkable. The values obtained with the hyperspherical data are almost always within the error bars of the measured parameters. In this energy region the agreement with the R -matrix results is not as good, but still the trend in relative signs and magnitudes is preserved. In general both A and B R -matrix parameters are lower in absolute value than the experimental ones. The comparison between the theoretical and experimental A and B parameters above the $3s8p$ resonance is done only for the R -matrix calculation because we could not fit the digitized hyperspherical data. For these higher resonances the agreement is again, very good. The predicted overall trend in relative signs and magnitudes, which is responsible for the actual line shapes, is confirmed by our experimental results.

It is interesting to analyze in some detail these parameters in the region of interaction between the $3snp$ series and the $3p4s$ interloper. This is the region between the $3s4p$ and $3s6p$ resonances. Theory predicts first a decrease in the resonance width going into the $3s4p$ resonance, and then a steady increase up to the $3s6p$ resonance, and we observe these effects in our data.

TABLE III. Quantum defect δ of the $3snp$ Rydberg series derived from our resonance positions and comparison with the results of the ion yield experiment [22] and theory.

| n | Experiment | | Theory | |
|-----|------------|----------------|--------------------------------|-----------------------------|
| | This work | Reference [22] | Hyperspherical, Reference [11] | R -matrix, Reference [12] |
| 3 | 0.714(2) | 0.706(3) | 0.716 | 0.697 |
| 4 | 0.927(4) | 0.919(5) | 0.939 | 0.855 |
| 5 | 0.378(11) | 0.338(9) | 0.400 | 0.149 |
| 6 | 0.550(18) | 0.469(7) | 0.626 | 0.299 |
| 7 | 0.720(28) | 0.631(20) | 0.801 | 0.466 |
| 8 | 0.794(43) | 0.64(13) | 0.928 | 0.589 |
| 9 | 0.912(61) | 0.92(26) | 1.119 | 0.656 |
| 10 | 0.84(9) | | 1.003 | 0.804 |
| 11 | 0.85(13) | | 1.109 | 1.033 |

With the resonance energies and the $3s$ threshold in Table I we obtained the quantum defects for all members of the $3snp$ series. The results are presented in Table III. There is, again, very good agreement between our results and those of Yoshida *et al.* [22]. The agreement with the hyperspherical results referred to the experimental $3s$ threshold [11] is also very good. The agreement with the R -matrix results [12] is better once the resonance energies are corrected for the $3s$ threshold. At the $3s3p$ resonance theory predicts a quantum defect close to 0.7 in agreement with experiment. Then it increases for the $3s4p$ resonance in both experiment and theory, and it drops at the $3s5p$ resonance due to the interaction with the $3p4s$ interloper. Experiment indicates a small rise in the quantum defect as one moves from the $6p$ to the $7p$ resonance, and then it stays very much constant. The calculations give a steady increase in the quantum defect. The hyperspherical calculation then gives an almost constant quantum defect of 1 while the R -matrix calculation predicts a jump in quantum defect at the $3s11p$ resonance. This is due to the effect of the $3d4p$ second interloper. In our experiment we find that if there is any effect, it is a drop in the quantum defect from 0.91 to 0.84, which is more in agreement with the behavior predicted by the hyperspherical calculation and goes in the opposite direction to the changes predicted by the R -matrix calculation. These measured variations are definitely too small to give conclusive evidence of the presence of the second interloper.

Our high resolution allowed us to measure the $2s$ relative partial cross section between the $3s$ and the $3p$ thresholds. In this energy region there are several series of resonances. There are the $3pns$ and $3pnd$ series converging to the $3p$ threshold, and there are several members of the $3dnp$ and $3dnf$ resonances in this energy region. The R -matrix calculation [12] has results for the resonance energies and also for the total and partial absorption cross sections. A comparison between our measurements and the R -matrix calculation is presented in Fig. 4. In the lower panel we give both the CIS results of the SS-Seya run (open triangles) and the PGM run (open circles), and also show with lines the result of a five point smoothing of the experimental data. In the upper panel we compare these smoothed data with the R -matrix results

for the $2s$ cross section. We show the original theoretical data (dashed lines) and the result of a convolution with a 7.5 meV bandpass window function (solid line). The theoretical data and resonance positions were shifted upwards by 17.7 meV.

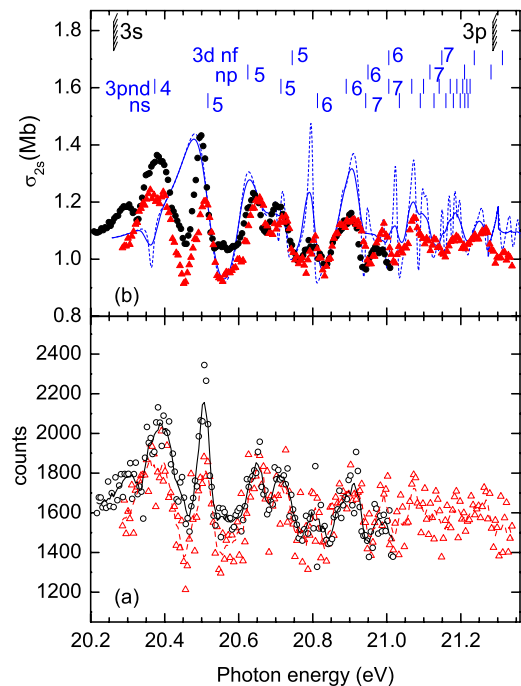


FIG. 4. (Color online) Autoionizing resonances between the $3s$ and $3p$ thresholds in atomic beryllium. Lower panel: Experimental results. Open triangles (red): CIS spectrum of the SS-Seya run (see text). Open circles (black): CIS spectrum of the PGM run. Dashed line (red): Result of a five-point smoothing of SS-Seya data. Solid line (black): Result of a five-point smoothing of PGM data. Upper panel: Filled circles (black): five-point smoothing of experimental PGM data normalized to cross section. Filled triangles: smoothed and normalized SS-Seya data. Solid line (blue): R -matrix results [12] convoluted with a 7.5 meV window function. Dashed line (blue): R -matrix results [12] with no convolution. The resonance energies are indicated as vertical lines and were taken from the R -matrix results shifted up by 17 meV (see text). The $3s$ and $3p$ thresholds (black) are taken from NIST [29].

This is the difference between the experimental [29] and the theoretical [12] $3p$ thresholds in Table I. Here we remark that according to the data in Fig. 2 right at the $3s$ threshold the PGM data are slightly above the SS-Seya data, and these are slightly higher than the R -matrix calculated cross section. In order to make a comparison among the data we decided to calculate new normalization factors in the energy region between the $3s$ and $3p$ thresholds. One factor minimizes the deviations at the $3s$ threshold of the PGM data from the calculation, the other factor does the same for the SS-Seya data.

First of all we point out that even though the scatter in the experimental data is large there is remarkable agreement between both smoothed curves. The PGM data seems to be riding, however, on a slightly negative slope, while the SS-Seya data seems to be riding on a flat continuum cross section. The overall agreement between experiment and theory is also rather good. The main discrepancy occurs at the first resonance ($3p4d$) in the group, near 20.36 eV. The R -matrix calculation predicts a dip in the cross section while we observe an excursion that peaks at a slightly higher photon energy. The cross section then goes through another maximum at the $3p5s$ resonance, at 20.50 eV, in close agreement with theory. Then we observe a double peak that according to theory consists of the $3p5d$ and $3d5s$ resonances. The calculation also gives a double peak, but with the dip slightly shifted to higher energies. There is also agreement between experiment and theory for the position of the $3p6s$ resonance (20.8 eV), even though the experimental width appears slightly larger. The agreement persists up to the $3p$ threshold even for our low resolution SS-Seya data. In this region between the $3s$ and $3p$ thresholds theory indicates that there are several resonances interacting with each other. This made us decide not to attempt any fits in this region of the spectrum. However, the qualitative agreement between experiment and theory allows us to conclude that, once again, most of the behavior of the total photoionization cross section is in the $2s$ partial channel.

IV. CONCLUSIONS

We presented results for the Be^{+2s} relative cross section between the $2p$ and $3p$ thresholds. Below the $3s$ threshold our high resolution allowed us to measure the parameters of the $3snp$ Rydberg series up to the $11p$ resonance. We compared these results with the ion yield measurements of the total cross section, and also with calculations for the $2s$ partial cross section. In general we found good agreement between experiment and theory. We confirmed the ion results [22] that the $3s5p$ and $3s6p$ resonances are strongly perturbed by the $3p4s$ interloper. The overall line shape due to this interaction is the same in the total and in the $2s$ partial cross section, indicating that the contribution of the $2p$ channel is not as strong at the resonances. The effect of the interloper is better modeled by the hyperspherical close coupling approximation [11]. There is also good agreement for the resonance energies once all results are referred to the NIST values [29].

In the region between the $3s$ and $3p$ thresholds we found good qualitative agreement between our $2s$ photoelectron cross section measurement and the calculation in the R -matrix approximation.

It is expected that these results will stimulate calculations searching for a better understanding of the correlation phenomena and autoionization in this relatively simple atomic system.

ACKNOWLEDGMENTS

This work is based in part upon research conducted at the Synchrotron Radiation Center, University of Wisconsin-Madison, which is supported by the National Science Foundation under Grant No. DMR-0537588. This work was partially supported by CONACyT, México, under project No. U41007-F. We want to thank Dr. D.-S. Kim and Professor S. T. Manson for providing us with their R -matrix data.

-
- [1] M. O. Krause and C. D. Caldwell, Phys. Rev. Lett. **59**, 2736 (1987).
 - [2] H. P. Kelly, Phys. Rev. A **9**, 1582 (1974).
 - [3] H. P. Saha and C. D. Caldwell, Phys. Rev. A **40**, 7020 (1989).
 - [4] L. VoKy, H. E. Saraph, W. Eissner, Z. W. Liu, and H. P. Kelly, Phys. Rev. A **46**, 3945 (1992).
 - [5] P. L. Altick, Phys. Rev. **169**, 21 (1968).
 - [6] C. H. Greene, Phys. Rev. A **23**, 661 (1981).
 - [7] P. F. O'Mahony and C. H. Greene, Phys. Rev. A **31**, 250 (1985).
 - [8] V. Radojevic and W. R. Johnson, Phys. Rev. A **31**, 2991 (1985).
 - [9] J. A. Tully, M. J. Seaton, and K. A. Berrington, J. Phys. B **23**, 3811 (1990).
 - [10] H.-C. Chi, K.-N. Huang, and K. T. Cheng, Phys. Rev. A **43**, 2542 (1991).
 - [11] B. Zhou and C. D. Lin, Phys. Rev. A **51**, 1286 (1995).
 - [12] D. S. Kim, S. S. Tayal, H.-L. Zhou, and S. T. Manson, Phys. Rev. A **61**, 062701 (2000).
 - [13] M. Rødbro, R. Bruch, and P. Bisgaard, J. Phys. B **12**, 2413 (1979).
 - [14] J. M. Esteva, G. Mehlman-Balloffet, and J. Romand, J. Quant. Spectrosc. Radiat. Transf. **12**, 1291 (1972).
 - [15] G. Mehlman and J. M. Esteva, Astrophys. J. **188**, 191 (1974).
 - [16] E. Jannitti, P. Nicolosi, and G. Tondello, Phys. Scr. **36**, 93 (1987).
 - [17] E. Jannitti, P. Nicolosi, G. Tondello, Z. Yongzhen, and M. Mazzoni, Opt. Commun. **63**, 37 (1987).
 - [18] R. Wehlitz and S. B. Whitfield, J. Phys. B **34**, L719 (2001).
 - [19] R. Wehlitz, D. Lukic, and J. B. Bluett, Phys. Rev. A **68**, 052708 (2003).
 - [20] D. Lukic, J. B. Bluett, and R. Wehlitz, Phys. Rev. Lett. **93**, 023003 (2004).
 - [21] R. Wehlitz, D. Lukic, and J. B. Bluett, Phys. Rev. A **71**,

- 012707 (2005).
- [22] F. Yoshida, L. Matsuoka, H. Osaki, S. Kikkawa, Y. Fukushima, T. Nagata, Y. Azuma, S. Obara, and S. Hasegawa, *Phys. Rev. A* **73**, 042709 (2006).
- [23] F. Yoshida, L. Matsuoka, R. Takashima, T. Nagata, Y. Azuma, S. Obara, F. Koike, and S. Hasegawa, *Phys. Rev. A* **73**, 062709 (2006).
- [24] S. Hasegawa, E. Recami, F. Yoshida, L. Matsuoka, F. Koike, S. Fritzsche, S. Obara, Y. Azuma, and T. Nagata, *Phys. Rev. Lett.* **97**, 023001 (2006).
- [25] F. Yoshida, F. Koike, S. Obara, Y. Azuma, T. Nagata, and S. Hasegawa, *Phys. Rev. A* **75**, 012714 (2007).
- [26] C. D. Caldwell, M. G. Flemming, M. O. Krause, P. van der Meulen, C. Pan, and A. F. Starace, *Phys. Rev. A* **41**, 542 (1990).
- [27] J. Jiménez-Mier, S. Schaphorst, C. D. Caldwell, and M. O. Krause, *J. Phys. B* **32**, 4301 (1999).
- [28] J. Jiménez-Mier, S. B. Whitfield, R. Wehlitz, and H. Díaz-Jiménez, *J. Phys. B* **34**, L693 (2001).
- [29] Yu. Ralchenko, F.-C. Jou, D. E. Kelleher, A. E. Kramida, A. Musgrove, J. Reader, W. L. Wiese, and K. Olsen, *NIST Atomic Spectra Database*, Version 3.1.2 (National Institute of Standards and Technology, Gaithersburg, MD, 2007); <http://physics.nist.gov/asd3>
- [30] B. W. Shore, *Phys. Rev.* **171**, 43 (1968).
- [31] A. F. Starace, *Phys. Rev. A* **16**, 231 (1977).
- [32] M. Koike, in *Vacuum Ultraviolet Spectroscopy II*, edited by J. A. Samson, and D. L. Ederer (Academic Press, San Diego, 1998), pp. 1–19.
- [33] R. Reininger, S. L. Crossley, M. A. Lagergren, M. C. Severnson, and R. W. C. Hansen, *Nucl. Instrum. Methods Phys. Res. A* **347**, 304 (1994).
- [34] S. B. Whitfield, R. Wehlitz, and M. Martins, *Radiat. Phys. Chem.* **70**, 3 (2004).
- [35] J. Cooper, and R. N. Zare, in *Lectures in Theoretical Physics*, S. Geltman, K. T. Mahanthappa, and W. E. Britten (Gordon and Breach, New York, 1969), Vol. XI-C, pp. 317–337.
- [36] S. B. Whitfield, R. Wehlitz, H. R. Varma, T. Banerjee, P. C. Deshmukh, and S. T. Manson, *J. Phys. B* **39**, L335 (2006).
- [37] M. O. Krause (unpublished).
- [38] S. B. Whitfield, M. O. Krause, P. van der Meulen, and C. D. Caldwell, *Phys. Rev. A* **50**, 1269 (1994).
- [39] C. N. Liu, and A. F. Starace, *Phys. Rev. A* **59**, R1731 (1999).
- [40] S. E. Canton-Rogan, A. A. Wills, T. W. Gorczyca, M. Wiedenhoef, O. Nayandin, Chien-Nan Liu, and N. Berrah, *Phys. Rev. Lett.* **85**, 3113 (2000).
- [41] J. Jiménez-Mier, *J. Quant. Spectrosc. Radiat. Transf.* **54**, 741 (1994).